Oxygen reduction reaction on electrodeposited PtAu alloy catalysts in the presence of phosphoric acid

Ji-Eun Lim [a],[1], Uk Jae Lee [a],[1], Sang Hyun Ahn [b], EunAe Cho [c], Hyoung-Juhn Kim [b], Jong Hyun Jang [b], Hyungbin Son [a],*, Soo-Kil Kim [a],*

[a] School of Integrative Engineering, Chung-Ang University, Heukseokno 84, Dongjak-gu, Seoul 156-756, Republic of Korea
[b] Fuel Cell Research Center, Korea Institute of Science and Technology, Hwarangno 14-gil 5, Seongbuk-gu, Seoul 136-791, Republic of Korea
[c] Department of Materials Science and Engineering, Korea Advanced Institute of Science and Technology (KAIST), 291 Daehak-ro, Yuseong-gu, Daejeon 305-701, Republic of Korea

ABSTRACT

We have investigated phosphate adsorption on the Au surface by in situ electrochemical surface-enhanced Raman spectroscopy to assess the possible use of Au-based alloys as catalysts for the oxygen reduction reaction (ORR) in high-temperature proton exchange membrane fuel cells. Compared with its strong adsorption in neutral or basic electrolytes, the adsorption of phosphate species on the Au surface were significantly altered in acidic electrolyte. Thus, Pt_xAu_{100-x} catalysts of various compositions were prepared by electrodeposition and exhibited better ORR activities than pure Pt in phosphoric acid electrolyte, which can be explained in terms of alloying effects and the different phosphate adsorption behavior.

© 2014 Elsevier B.V. All rights reserved.

1. Introduction

The use of proton exchange membrane fuel cells (PEMFCs) has been recognized as a highly efficient and environmentally friendly method for the utilization of hydrogen [1]. Under relatively high temperature operation of PEMFCs (over 120 °C), several advantages are expected, mostly in terms of the enhanced kinetics of both the anodic and cathodic reactions [2]. Moreover, the allowance for a higher level of CO in the reformed hydrogen leads to improved durability as well as reduced fabrication costs by eliminating the CO-removal step [3]. However, operation temperatures higher than 100 °C require membrane types other than conventional perfluorosulfonic acid (PFSA)-based membranes such as Nafion because of the vaporization of water and consequential loss of proton conductivity [4]. Instead, a phosphoric acid (PA)-doped polybenzimidazole (PBI) membrane has been adopted as an alternative electrolyte for high-temperature PEMFCs [5–7]. Nevertheless, there is still a serious drawback to the employment of a PA–impregnated membrane: the significant degradation of the Pt

catalyst by the strong adsorption of phosphate on the Pt surface, blocking the catalyst active sites [8].

The adsorption behavior of phosphate species on the Pt surface has been investigated by various spectroscopic and electrochemical methods [9–11]. In aqueous solution, the phosphate species conceivably exist as molecular H_3PO_4 as well as $H_2PO_4^-$, HPO_4^{2-}, and PO_4^{3-} ions [9–11]. Among these, the $H_2PO_4^-$ ion is the strongest adsorbate on the Pt surface, although this depends on the pH, phosphate concentration, and Pt crystal orientation [12]. On the other hand, there is controversy regarding the adsorption behavior of phosphate species on the Au surface. Habib et al. [9] performed a Fourier-transform infrared (FTIR) study of the adsorption from aqueous solutions of phosphoric acid onto Pt and Au surfaces at various concentrations and potentials, and their results suggested that molecular H_3PO_4 is more strongly adsorbed on the Au surface than on the Pt surface in acidic solutions, although it is not conclusive due to the lack of calibrations. Niaura et al. [10] employed electrochemical surface-enhanced Raman spectroscopy (EC-SERS) to investigate the adsorption of phosphate ion species on Ag, Au, and Cu surfaces, and found that SER spectra on Au are only observed in alkaline solutions. The SER spectra show evidence of the adsorption of phosphate ions in alkaline solutions, but there are no data to determine the adsorption behavior of phosphate species in acidic solutions. This could be because EC-SERS is more sensitive to the

species very close to the metallic surface (<10 nm) than FTIR which is also sensitive to species in the bulk solution in the IR beam path. Webber et al. [11] state that to prevent this "bulk effect" when using FTIR, a carefully designed solution is needed.

In this work, to study the adsorption behavior of phosphate ion species on Au surfaces under various pH conditions, the EC-SERS technique was used. Raman spectra on the Au surface were obtained during cyclic voltammetry scans, providing in situ information about the chemical state of the electrode surface, including the oxidation state of the electrode and the identity of the adsorbed chemical species. Although a previous study showed that EC-SERS could be used to identify the adsorption state of phosphate species on an Au electrode in basic solutions [10], the results could not be used directly in the interpretation of PA behaviors under the highly acidic PEMFC operating conditions.

Along with Pt, Au has been considered as an attractive material for improving the activity and stability of Pt catalysts for the oxidations of hydrogen [13], alcohols [14,15], and formic acid [16,17] as well as the ORR [18–22]. In particular, in the ORR with a PA-free electrolyte, various approaches have been taken to prepare Pt–Au bimetallic catalysts such as Au-cluster-decorated Pt nanoparticles [19,20], Au@Pt dendrimer-encapsulated nanoparticles [21], and Pt–Au alloys [22–24]. For example, Zhang et al. [19] reported Pt nanoparticles modified with Au clusters (Au/Pt/C), which demonstrated extremely high stability over 30,000 cycles while continuously exhibiting a specific kinetic current density comparable to that of the Pt/C catalyst. This enhanced durability is described by the higher oxidation potential of Au-modified Pt. An increase in the ORR performance was even observed in the case of PtAu bimetallic catalysts [20] despite the inactivity of Au for the ORR [25]. Hu et al. [23] reported the improved ORR activity of electrodeposited PtAu than that of pure Pt and explained it in terms of Au role as a Pt—OH bond breaker. Luo et al. [24] demonstrated the synthesis of carbon supported PtAu catalysts for ORR application in alkaline electrolyte. The synergistic effect of PtAu

was tried to be explained with adsorption of oxygenated species on Au.

From this discussion, the Pt–Au bimetallic structure and/or PtAu alloys can be considered as potential catalysts for the ORR. However, as far as we know, studies on the effect of the composition and structure of PtAu alloys on the ORR activity in the presence of PA are scarce. Lee et al. [26] has reported slightly enhanced tolerance of the Au_{core}–Pt_{shell}/C catalyst toward phosphate adsorption than the Pt/C catalyst, while the mass activities were similar. However, lack of knowledge about the adsorption of PA on the Au surface inhibits a better understanding of the ORR activity of PtAu catalysts in the presence of PA. Therefore, in situ EC-SERS was adopted to study the behavior of PA on the Au surface. Then, the performance of composition-controlled PtAu alloy catalysts for the ORR in the presence of PA was assessed.

2. Experimental

The EC-SERS experiment was performed using an in situ electrochemical cell consisting of a platinum mesh counter electrode, a Ag/AgCl reference electrode, and a Au-coated SERS working electrode (Klarite, Renishaw Inc.), placed on the stage of a commercial micro-Raman instrument (XperRam 200, Nanobase) (Fig. 1). Three different phosphate solutions (pH 2.2, 7.2, and 9.0) were prepared by adding different concentrations of either 100 mL NaOH solution or 100 mL HClO$_4$ solution, as pH adjusters, to 100 mL 0.1 M NaH$_2$PO$_4$ solution. Total phosphate concentrations were kept to be 0.05 M in the final solution. The potential of the working electrode (E) was measured against the reference electrode and converted versus the reversible hydrogen electrode (RHE). The potential range for cyclic voltammetry (CV) was 0.32 to 1.58 V$_{RHE}$ at a scan rate of 50 mV s^{-1}.

SER spectra were collected using a 641-nm laser source with an incident power of 15 mW at the working electrode surface. A low-magnification objective (10×, 0.25NA Olympus) was used to
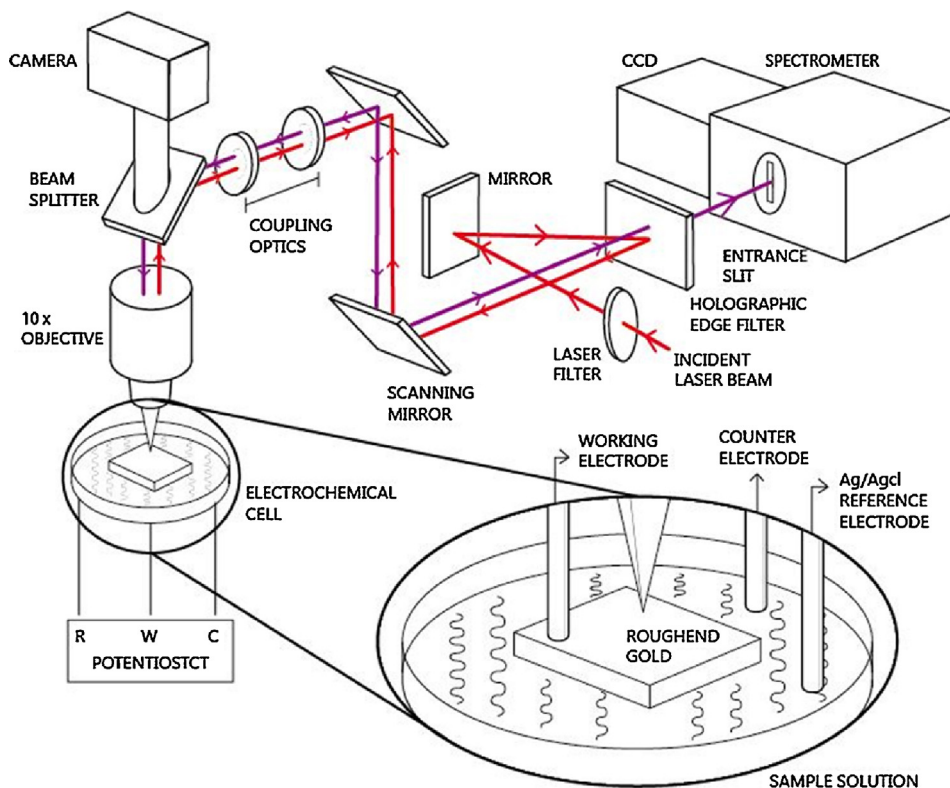

Fig. 1. Schematic of EC-SERS setup. A red laser (641 nm) is used to obtain SER spectra from a roughened gold substrate during cyclic voltammetry scans. An in situ electrochemical cell is placed under a low-magnification objective (10×) for Raman acquisition in backscattering geometry.

focus the laser to a spot of ≈3 μm. The exposure time was set to 500 ms so that one SER spectrum covered a potential sweep range of 25 mV. The SER spectra were collected from each solution while the CV scan was run for 20 cycles.

For the Pt electrodeposition, the electrolyte containing 10 mM $H_2PtCl_6 \cdot xH_2O$ supported by 0.5 M NaCl was prepared. For the preparation of composition-controlled PtAu alloys, $HAuCl_4 \cdot xH_2O$ was added to the electrolyte in various concentrations from 1 to 7 mM. After Ar purging to remove the dissolved oxygen from the electrolytes, the electrodepositions of Pt and the PtAu alloys were carried out with a conventional three-electrode cell consisting of a glassy carbon (GC) rotating disk electrode (RDE) as the working electrode, a Pt sheet as the counter electrode, and Ag/AgCl/saturated KCl as the reference electrode. The deposition potential was fixed at −0.3 V for 20 min, and was controlled with a potentiostat (Autolab, PGSTAT302F). The prepared deposits were further subjected to electrochemical analysis.

For spectroscopic characterization of the electrodeposited Pt and PtAu alloy catalysts, the same electrodeposition was performed on GC films purchased from HTW (Sigradur). GC films were used instead of the GC RDE because it was not feasible to use the RDE in the chambers of the spectroscopic analysis equipment. The morphologies were observed by field-emission scanning electron microscopy (FESEM, JEOL, JSM-6700F). The compositions of the PtAu alloys were measured by energy dispersive spectroscopy (EDS, JEOL, JSM-6700F). Crystallographic analysis of the electrodeposits was performed by X-ray diffraction (XRD, Bruker-AXS, New D8-Advance) with a scan rate of $5° \, \text{min}^{-1}$.

The catalytic activities toward the ORR were tested by using linear sweep voltammetry (LSV) in the potential range $1.05–0.05 \, V_{RHE}$ at a scan rate of $5 \, \text{mV} \, \text{s}^{-1}$. The electrodeposited catalyst on the GC RDE was used as the working electrode with a rotation rate of 1500 rpm. The electrolytes containing 0.1 M $HClO_4$, with or without

0.1 M H_3PO_4, were purged continuously with O_2 before and during measurement.

The electrochemical behaviors of the catalysts were also investigated by measuring their CVs in the potential range $0–1.2 \, V_{RHE}$ at a scan rate of $50 \, \text{mV} \, \text{s}^{-1}$ in 0.1 M $HClO_4$ with or without 0.1 M H_3PO_4. The electrolytes were deaerated with Ar purging for 60 min. The potential range was configured with Ag/AgCl/saturated KCl, and then converted to the RHE. All the electrochemical measurements were performed at 298 K.

3. Results and discussion

SER spectra collected during CV in the 1st, 10th, and 20th cycles are illustrated in Figs. 2a–c, 3a–c, and 4a–c, respectively. The corresponding CVs in the three phosphate solutions with different pH are shown in Figs. 2d, 3d, and 4d, respectively. The CV scans in the 1st cycle (Fig. 2d) show that the formation of a surface compound is initiated slowly from approximately $E = 1.2 \, V_{RHE}$ during the positive sweep. The reduction occurs more abruptly during the negative sweep at approximately $E_{peak} = 0.85 \, V_{RHE}$. This result is consistent with the SER spectra (Fig. 2a–c), in which a broad peak at $580 \, \text{cm}^{-1}$ starts to appear when the potential becomes $E = 1.3 \, V_{RHE}$ during the positive sweep and disappears when E drops below $0.8 \, V_{RHE}$ in the negative sweep. This peak at $580 \, \text{cm}^{-1}$ has previously been assigned to Au—OH [10]. Neither the CVs nor the SER spectra show evidence of the adsorption of phosphate species, regardless of solution pH.

A comparison of the CVs at the 10th (Fig. 3d) with that at the 1st cycle (Fig. 2d) shows an additional peak at $E = 0.8–1.0 \, V_{RHE}$ in the pH 9 solution but not in the other solutions. The SER spectra in the same solution (Fig. 3a) show strong peaks at $≈795 \, \text{cm}^{-1}$ and $≈930 \, \text{cm}^{-1}$ and a weaker peak at $≈1095 \, \text{cm}^{-1}$ from $E = 0.7–1.2 \, V_{RHE}$ during the positive sweep and $E = 0.8–0.6 \, V_{RHE}$ during the negative
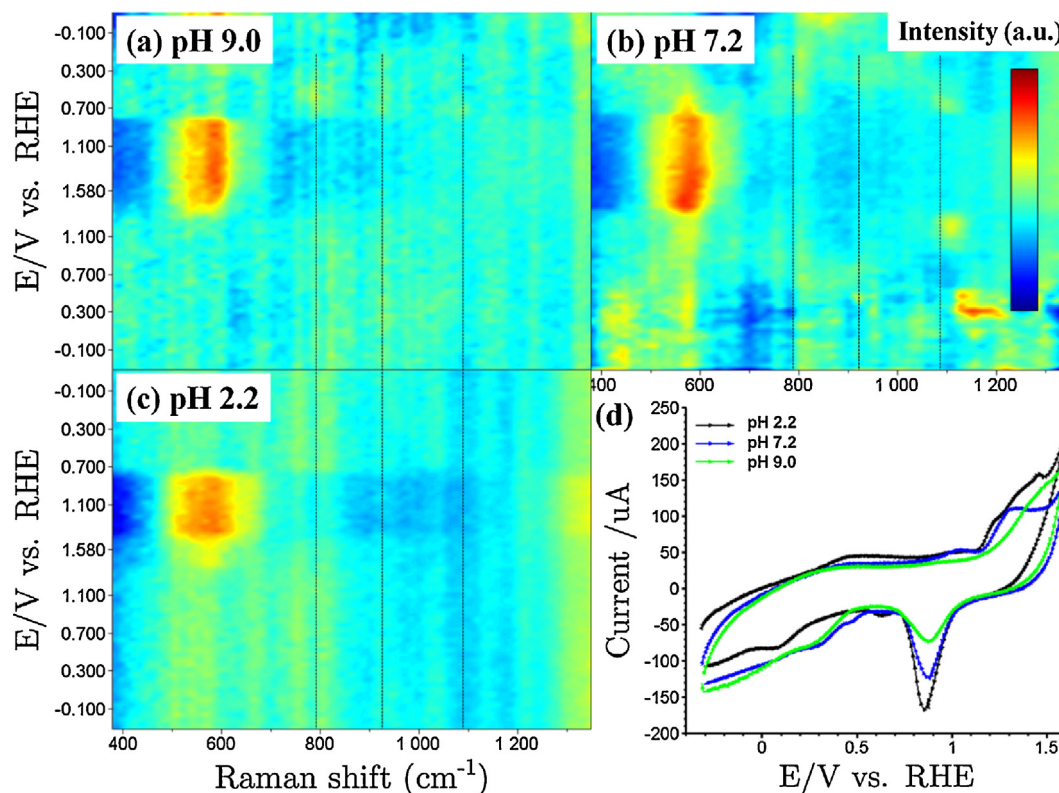

Fig. 2. Sequence of SER spectra obtained during cyclic voltammetric scans at a roughened Au electrode (Klarite) during the 1st CV cycle in (a) pH 9.0, (b) pH 7.2, and (c) pH 2.2 solutions. The vertical axis shows the potential of the working electrode versus RHE. The dotted vertical lines indicate the peak locations of adsorbed phosphate species. The CV sweep direction is from bottom to top. The respective cyclic voltammograms during the Raman acquisitions are shown in (d). The scan rate was $50 \, \text{mV} \, \text{s}^{-1}$.
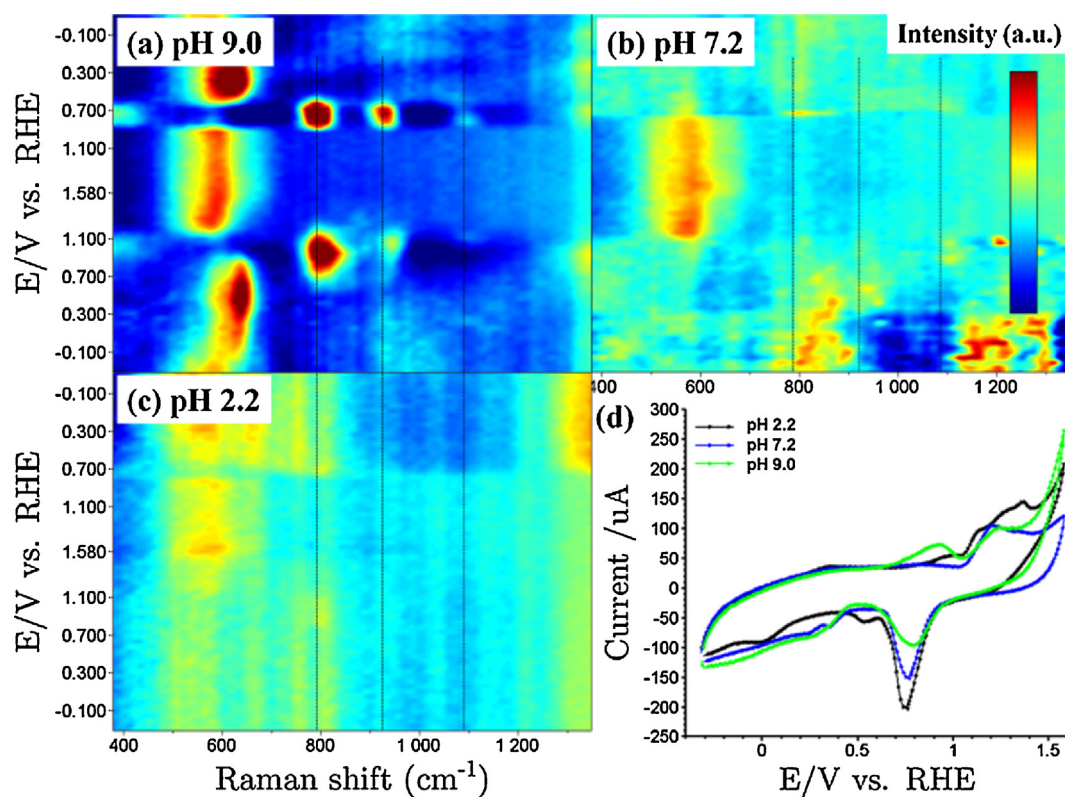
Fig. 3. Sequence of SER spectra obtained during cyclic voltammetric scans at a roughened Au electrode (Klarite) during the 10th CV cycle. For detailed description, see the caption of Fig. 2.
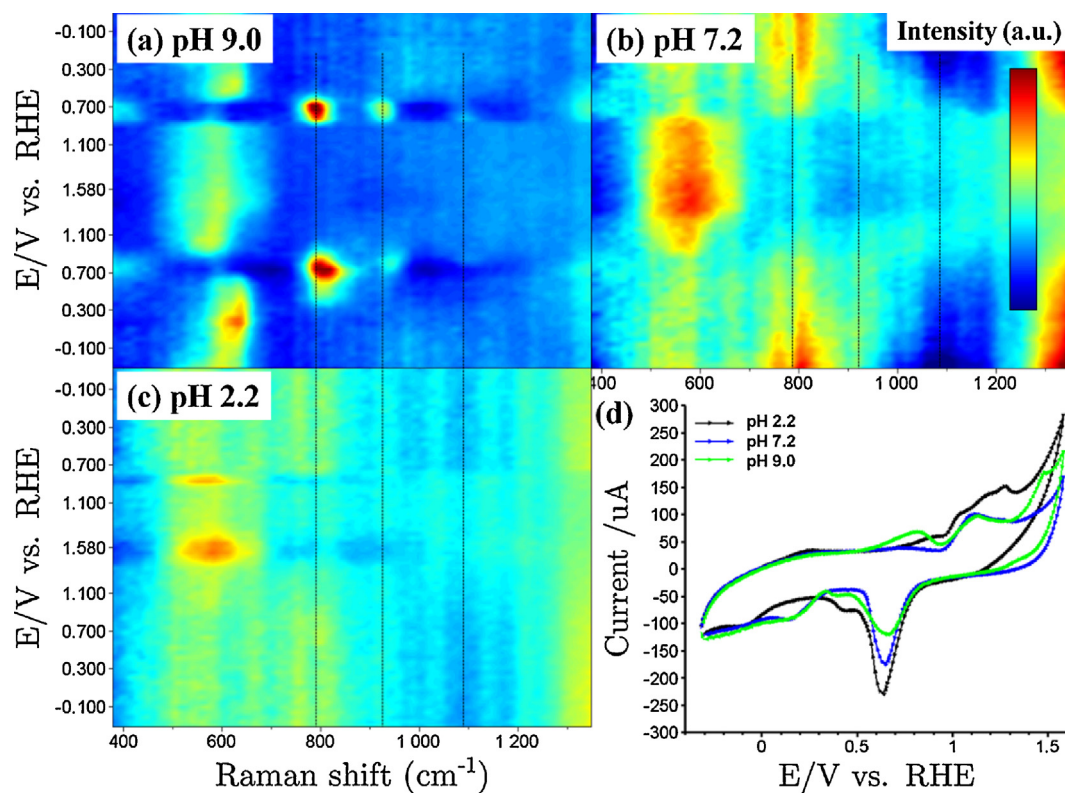

Fig. 4. Sequence of SER spectra obtained during cyclic voltammetric scans at a roughened Au electrode (Klarite) during the 20th CV cycle. For detailed description, see the caption of Fig. 2.

sweep. The peaks at $\approx 930\,cm^{-1}$ and $\approx 1090\,cm^{-1}$ have previously been assigned to the vibrational modes of adsorbed phosphate species in monodentate geometry [10]. The peak at $795\,cm^{-1}$ which accompanies the peak at $\approx 930\,cm^{-1}$ has not been assigned in the previous EC-SERS study. This peak can be assigned to vibrational modes of the adsorbed phosphate ion species in bidentate geometry, whose structural configuration can be found in the literature [10]. As the Au—OH is formed at $E > 1.2\,V_{RHE}$ during the positive sweep, the SER signal of the phosphate ions disappears and Au—OH peak at $\approx 580\,cm^{-1}$ emerges. This result is fully consistent with a previous SERS study [10], and is in partial agreement with the adsorption behavior of molecular H_3PO_4 studied using FTIR [9]. One can identify similar peaks from the pH 7.2 solution (Fig. 3b), but the intensity is much weaker. In the pH 2.2 solution (Fig. 3c), only the Au—OH peak can be found; no peaks related to adsorbed phosphate species appear. The SER spectra and CVs of the 20th cycle (Fig. 4) are similar to those of the 10th cycle, with the only differences being in the intensities of the SER spectra. The fact that there are no phosphate peaks in Fig. 3c might be attributed to the dissolution of Au under acidic conditions. However, this is not likely, because the Au—OH peak was still observed and the corresponding CV in Fig. 3d exhibited similar shapes of Au redox reactions to those of Au at different pH values. The broad peak between $580\,cm^{-1}$ and $650\,cm^{-1}$ in Figs. 3a and 4a seems to be related to the Au—OH vibration and the

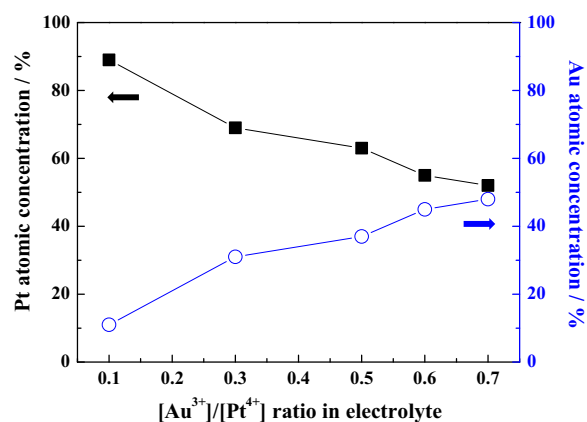**Fig. 5.** Atomic concentrations of Pt and Au in electrodeposited PtAu alloy catalysts as a function of $[Au^{3+}]/[Pt^{4+}]$ ratio in the electrolyte.

Au—O vibration, respectively [10]. However, the potential range for these peaks ($E < 0.8\,V_{RHE}$ during the positive sweep and $E < 0.6\,V_{RHE}$ during the negative sweep) is different with the reported one [10]. Thus, it is difficult to exactly assign the peaks, for the present.
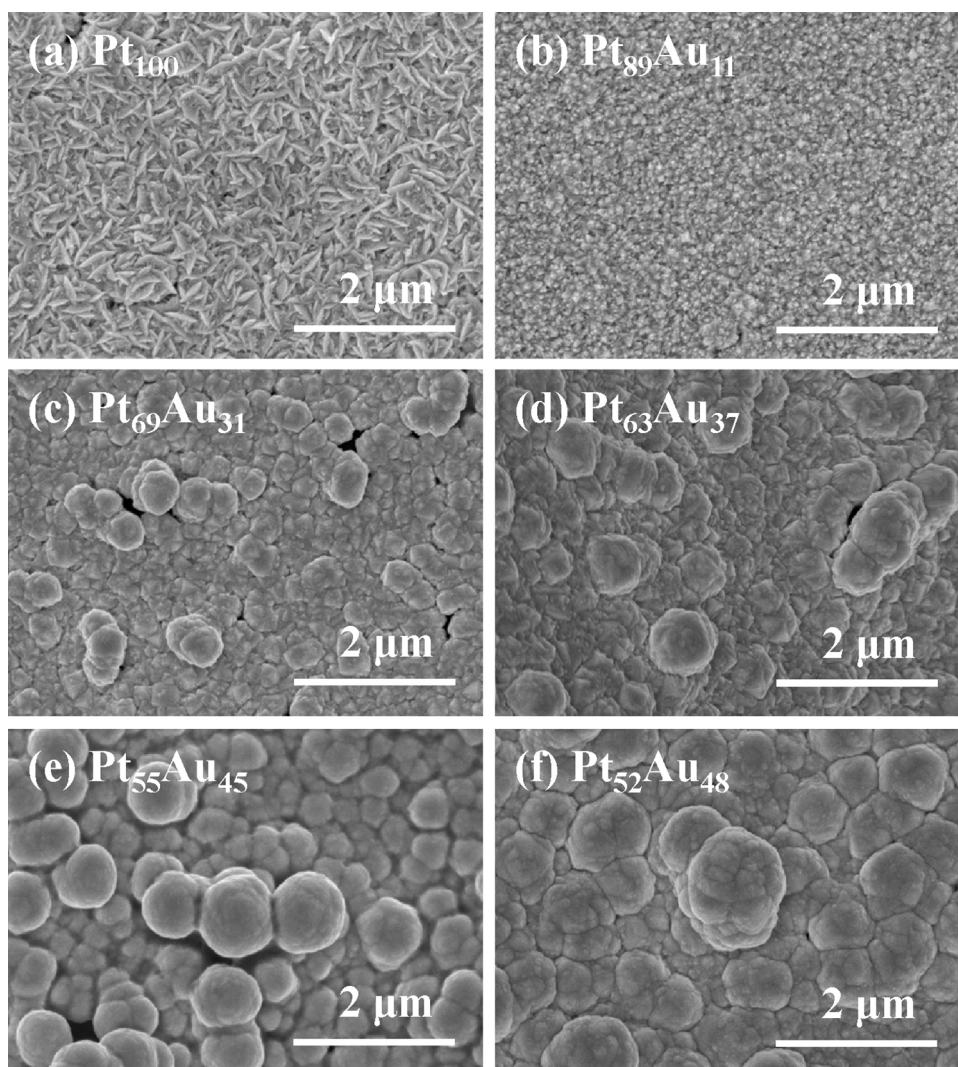

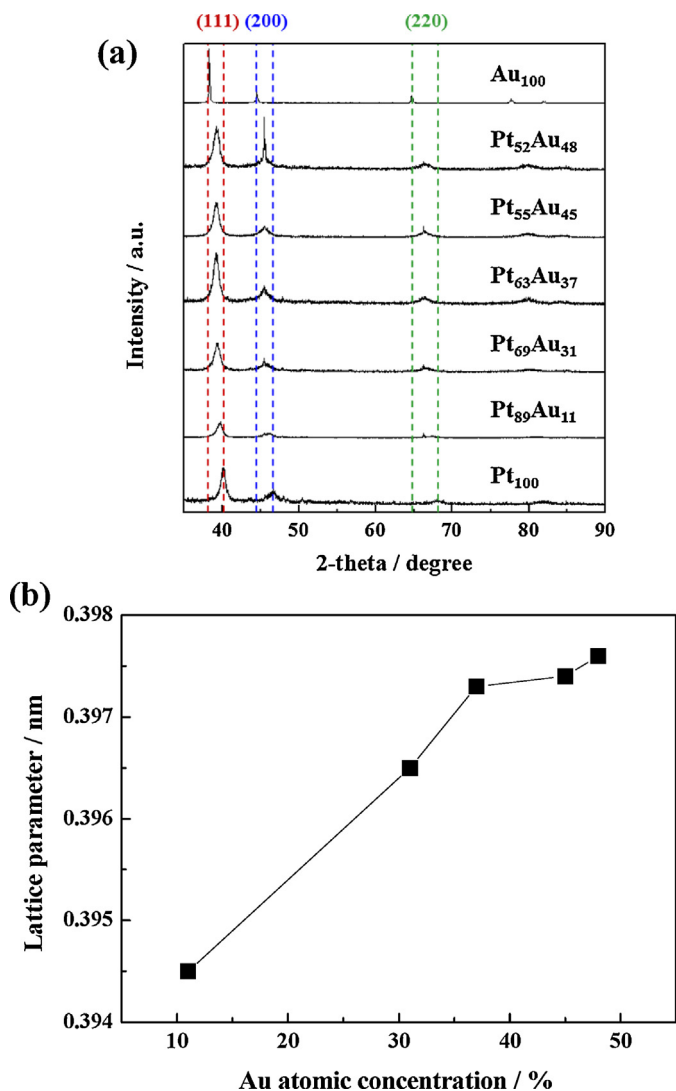**Fig. 6.** FESEM images of electrodeposited Pt and PtAu alloys.

Fig. 7. (a) XRD patterns of electrodeposited Pt, PtAu alloys, and Au and (b) Lattice parameters of electrodeposited PtAu alloys as a function of Au atomic concentration.

Motivated by the EC-SERS results on Au under acidic conditions, we prepared composition-controlled PtAu on glassy carbon substrates using electrodeposition methods at $-0.3\,V_{Ag/AgCl}$ for 20 min. The concentration ratio of the Au/Pt precursor was varied from 0.1 to 0.7 in 0.5 M NaCl supported electrolyte; therefore, the Au atomic compositions of the PtAu deposits increased gradually from 11% to 48% (Fig. 5). The electrodeposits are denoted as Pt_xAu_{100-x} according to their compositions. The morphology changes were monitored according to the compositional variation (Fig. 6). For the electrodeposited Pt_{100} (Fig. 6a) needle-like shapes were observed. With increasing Au composition in the PtAu deposits (Fig. 6b–f), the morphology changed from needle-like to large, agglomerate shapes, accompanied by a gradual increase in grain size. The crystal structures of the electrodeposits were also analyzed by XRD (Fig. 7a). The peak positions of (1 1 1), (2 0 0), and (2 2 0) for Pt_{100} were located at 40.2°, 46.7°, and 68.0°, respectively, whereas those for Au_{100} were observed at 38.3°, 44.5°, and 64.7°, respectively [27]. The peaks of (1 1 1), (2 0 0), and (2 2 0) for the PtAu deposits appeared between those for Pt_{100} and Au_{100}, confirming the formation of PtAu alloys. Evidently, with increasing Au composition in the PtAu alloys, the lattice parameters (Fig. 7b) increased.

Fig. 8a shows the polarization curves of the ORR for Pt_{100} and various PtAu alloy catalysts in O_2-saturated 0.1 M $HClO_4$.
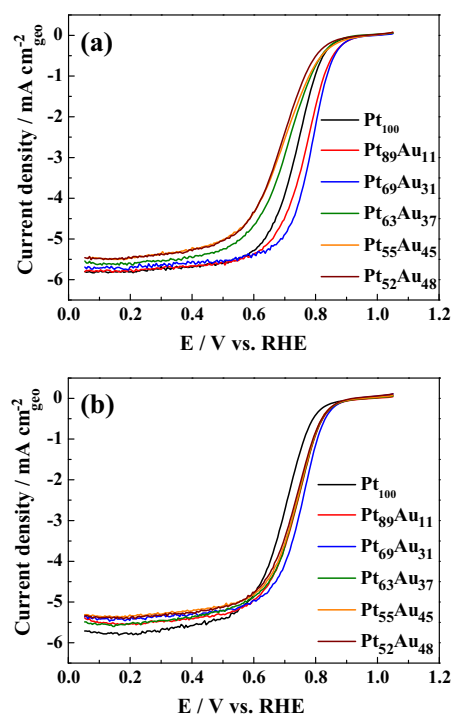

Fig. 8. Polarization curves for oxygen reduction reaction of Pt_{100} and various PtAu alloys in an O_2-saturated 0.1 M $HClO_4$ solution (a) without PA and (b) with PA (0.1 M). The scan rate was 50 mV s^{-1} and RDE velocity was 1500 rpm.

For the deposited pure Au (Au_{100}), a negligible activity for ORR was observed (not shown here). Without PA, the kinetic current density (Fig. 9a, normalized with respect to geometric electrode area) and mass activity (Fig. 9b, based on the total mass of Pt and Au) of the catalysts were significantly enhanced with increasing
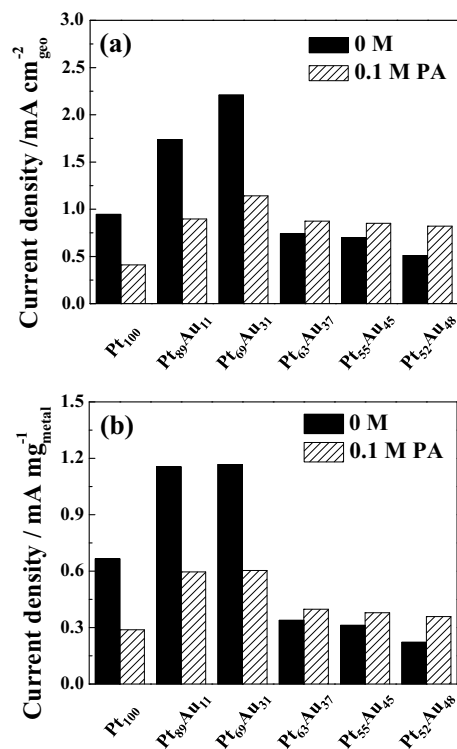

Fig. 9. Kinetic current densities of Pt_{100} and PtAu alloy catalysts based on (a) geometric surface area and (b) total metal mass for the ORR at 0.8 V_{RHE}.

Au composition in the catalysts from 0 (Pt_{100}) to 31% ($Pt_{69}Au_{31}$). Owing to the relatively bulky morphologies (Fig. 6), the activities of our electrodeposited catalysts are lower than those of conventional nanoparticle catalysts, and the activities are compared at 0.8 V_{RHE}, where the differences between the samples are more distinguishable. A further increase in Au composition (37–48%) decreased the ORR activity. Interestingly, alloying with Au below a certain content actually enhanced the ORR activity, though Au has been known to follow a two-electron process and be inactive toward the water-generating ORR [19]. Because the atomic size and electronegativity of Au are higher than those of Pt, alloys of Pt with Au are expected to have lower ORR activities than other PtM alloys (where M = Fe, Co, Ni, etc.). However, the high activity toward the ORR of Au-clustered Pt has been reported [19,20]. To explain this, Zhang et al. [19] suggested H_2O_2 spillover from Au to neighboring Pt and subsequent reduction to water, or aiding of the reduction of H_2O_2 by AuOH. Zhang et al. [20] insisted on a four-electron process on the Au surface without H_2O_2 production to explain the higher ORR activity of the PtAu/C catalyst. In accordance with those results, we observed an enhanced ORR activity for some PtAu alloys. It is also natural to comment on the morphologies of the PtAu alloys to explain the activity variations, but we do not do this here because we could not control the morphologies of the PtAu deposits, i.e., artificial fabrication of different morphologies with the same composition was not achievable. However, if the Au content was too high, the activity decreased; this is often observed in the case of alloy catalysts owing to the excess alternation of the electronic structure of Pt (or both of the components). Severe agglomerations at higher Au contents (Fig. 6) are also responsible for activity loss.

In the presence of 0.1 M PA in the $HClO_4$ electrolyte, the ORR activities changed significantly (Fig. 8b; the results are also summarized in Fig. 9a and b). With relatively low Au contents (0–31%), the ORR activities of Pt_{100}, $Pt_{89}Au_{11}$, and $Pt_{69}Au_{31}$ catalysts in the presence of PA decreased to roughly half their original activities, although the kinetic current density of the $Pt_{69}Au_{31}$ alloy catalyst with PA is still comparable to that of the Pt_{100} catalyst without PA. This implies that the inhibition of the adsorption of phosphate species on PtAu with relatively low amounts of Au was not significant, while the significant ORR activity of $Pt_{69}Au_{31}$ was attributed to the alloying effects. A more interesting phenomenon occurs at higher composition of Au: the ORR activities of PtAu with PA were even higher than those without PA. The reasons for this abnormal behavior at high Au contents are quite difficult to interpret, and there are some competing factors at play: (i) enhanced suppression of phosphate species adsorption at high Au contents, (ii) deterioration of ORR activity at high Au contents, and (iii) positive influence of PA on the ORR. Regarding the third factor, Habib and Bockris [9] once proposed the possibility of an increase in O_2 reduction activity by enhanced proton activity in the presence of another acid. They also commented on the enhanced resonance tunneling of electrons by adsorbed species. Park et al. [28] previously reported that the ORR activity of a Se-modified Ru catalyst was enhanced by PA addition (10 mM), which was explained by PA adsorption on the Se atoms and a resultant decrease in the oxygen binding energy on the Ru atoms. Alternatively, the adsorbed phosphate species may provide an electron to the catalysts, leading to an electron-enriched surface favorable for the ORR. Similarly, Park et al. [29,30] explained the enhanced ORR activity of $Au/AlPO_4$ nanocomposites by electron transfer from $AlPO_4$ to Au. However, most importantly, the PtAu alloy catalysts exhibited better activities than pure Pt (to a greater or lesser extent) when PA was present in the electrolyte.

The CVs of the Pt_{100} and $Pt_{52}Au_{48}$ catalysts were recorded in Ar-saturated $HClO_4$ with or without PA (Fig. 10a and b). For Pt_{100} with PA (Fig. 10a), clear adsorption and desorption peaks of PA on the Pt surface were observed at around 0.21 V_{RHE}, while the redox couple of PtOH formation and reduction was suppressed [26] owing to
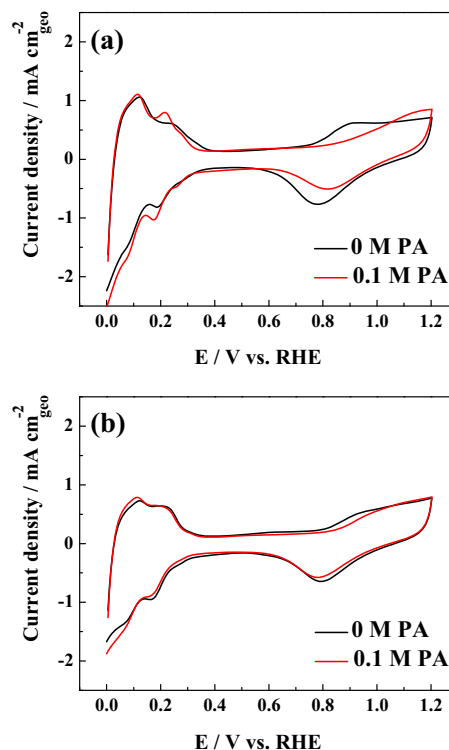

Fig. 10. CV curves of (c) Pt_{100} and (d) $Pt_{52}Au_{48}$ catalysts in $HClO_4$ electrolyte, with or without PA.

the competition between PA adsorption and the adsorption of oxygenated species. A similar observation was made for PtAu with low Au content. However, the $Pt_{52}Au_{48}$ alloy catalyst with PA (Fig. 10b) showed an almost identical CV to that without PA. The stabilization of Pt by Au [19] is responsible for the suppressed PtOH formation peak in the absence of PA at around 0.9 V.

4. Conclusions

PtAu alloy catalysts with different Au contents were fabricated by the electrodeposition process. In the presence of PA, the composition-controlled PtAu alloy catalysts demonstrated higher ORR activities than Pt. These interesting phenomena conceivably originated from the alloying effects with Au and the alteration of the adsorption of phosphate species, as confirmed by electrochemical analysis and in situ EC-SERS in acidic solution.

References

[1] M.K. Debe, Nature 486 (2012) 43–51.
[2] J. Zhang, Z. Xie, J. Zhang, Y. Tang, C. Song, T. Navessin, Z. Shi, D. Song, H. Wang, D.P. Wilkinson, Z. Liu, S. Holdcroft, J. Power Sources 160 (2006) 872–891.
[3] Y. Shao, G. Yin, Z. Wang, Y. Gao, J. Power Sources 167 (2007) 235–242.
[4] C. Yang, P. Costamagna, S. Srinivasan, J. Benziger, A.B. Bocarsly, J. Power Sources 103 (2001) 1–9.
[5] J.A. Asensio, E.M. Sánchez, P. Gómez-Romero, Chem. Soc. Rev. 39 (2010) 3210–3239.

[6] Q. Li, J.O. Jensen, R.F. Savinell, N.J. Bjerrum, Prog. Polym. Sci. 34 (2009) 449–477.
[7] B. Smitha, S. Sridhar, A.A. Khan, J. Membr. Sci. 259 (2005) 10–26.
[8] L. Qingfeng, H.A. Hjuler, N.J. Bjerrum, J. Appl. Electrochem. 31 (2001) 773–779.
[9] M.A. Habib, J.O'M. Bockris, J. Electrochem. Soc. 132 (1985) 108–114.
[10] G. Niaura, A.K. Gaigalas, V.L. Vilker, J. Phys. Chem. B 101 (1997) 9250–9262.
[11] M. Webber, F.C. Nart, Electrochim. Acta 41 (1996) 653–659.
[12] Q. He, X. Yang, W. Chen, S. Mukerjee, B. Koel, S. Chen, Phys. Chem. Chem. Phys. 12 (2010) 12544–12555.
[13] J. Solla-Gullón, A. Aldaz, J. Clavilier, Electrochim. Acta 87 (2013) 669–675.
[14] M. Li, P. Liu, R.R. Adzic, J. Phys. Chem. Lett. 3 (2012) 3480–3485.
[15] J. Kim, C. Jung, C.K. Rhee, T. Lim, Langmuir 23 (2007) 10831–10836.
[16] K. Kristian, Y. Yan, X. Wang, Chem. Commun. (2008) 353–355.
[17] M.D. Obradović, A.V. Tripković, S.L. Gojković, Electrochim. Acta 55 (2009) 204–209.
[18] Y. Bing, H. Liu, L. Zhang, D. Ghosh, J. Zhang, Chem. Soc. Rev. 39 (2010) 2184–2202.
[19] J. Zhang, K. Sasaki, E. Sutter, R.R. Adzic, Science 315 (2007) 220–222.
[20] Y. Zhang, Q. Huang, Z. Zou, J. Yang, W. Vogel, H. Yang, J. Phys. Chem. C 114 (2010) 6860–6868.
[21] D.F. Yancey, E.V. Carino, R.M. Crooks, J. Am. Chem. Soc. 132 (2010) 10988–10989.
[22] P. Hernández-Fernández, S. Rojas, P. Ocón, J.L.G. Fuente, J.S. Fabián, J. Sanza, M.A. Peña, F.J. Carcía-García, P. Terreros, J.L.G. Fierro, J. Phys. Chem. C 111 (2007) 2913–2923.
[23] Y. Hu, H. Zhang, P. Wu, H. Zhang, B. Zhou, C. Cai, Phys. Chem. Chem. Phys. 13 (2011) 4083–4094.
[24] J. Luo, P.N. Njoki, Y. Lin, L. Wang, C.J. Zhong, Electrochem. Commun. 8 (2006) 581–587.
[25] J.K. Nørskov, J. Rossmeisl, A. Logadottir, L. Lindqvist, J.R. Kitchin, T. Bligaard, H. Jónsson, J. Phys. Chem. B 108 (2004) 17886–17892.
[26] K.-S. Lee, S.J. Yoo, D. Ahn, S.-K. Kim, S.J. Hwang, Y.-E. Sung, H.-J. Kim, E. Cho, D. Henkensmeier, T.-H. Lim, J.H. Jang, Electrochim. Acta 56 (2011) 8802–8810.
[27] I.-S. Park, K.-S. Lee, D.-S. Jung, H.-Y. Park, Y.-E. Sung, Electrochim. Acta 52 (2007) 5599–5605.
[28] H.-Y. Park, S.J. Yoo, S.J. Kim, S.-Y. Lee, H.C. Ham, Y.-E. Sung, S.-K. Kim, S.J. Hwang, H.-J. Kim, E. Cho, D. Henkensmeier, S.W. Nam, T.-H. Lim, J.H. Jang, Electrochem. Commun. 27 (2013) 46–49.
[29] Y. Park, S. Nam, Y. Oh, H. Choi, J. Park, B. Park, J. Phys. Chem. C 115 (2011) 7092–7096.
[30] Y. Park, B. Lee, C. Kim, J. Kim, S. Nam, Y. Oh, B. Park, J. Phys. Chem. C 114 (2010) 3688–3692.